n-Octadecyltriethoxysilane Monolayer Coated Surfaces in Humid Atmospheres: Influence of Capillary Condensation on Surface Deformation and Adhesion

Sungsoo Kim,[†] Hugo K. Christenson,[‡] and Joan E. Curry*[,†]

Department of Soil, Water and Environmental Science, University of Arizona, Tucson, Arizona 85721, and Department of Physics and Astronomy, The University of Leeds, LEEDS LS2 9JT, United Kingdom

Received: July 24, 2002; In Final Form: February 11, 2003

We have investigated the effect of humidity on surface deformation and adhesion of mica surfaces coated with *n*-octadecyltriethoxysilane self-assembled monolayers using a surface forces apparatus. The Maugis model of contact elasticity based on linear elastic fracture mechanics is used to analyze the results. The Laplace pressure is assumed to act in the "Dugdale" zone outside the contact area to account for capillary condensation. We measure the radius of the contact area as a function of applied load and use the model to obtain the surface energy and elastic constant of these surfaces for humidities ranging from 0 to 99%. The limiting values in dry and near-saturated conditions are as expected from well-known theories. A significant result is that we also obtain the surface energy for intermediate humidities. Increasing humidity modifies the deformed shape of the surfaces in contact due to capillary condensation. The sharp bifurcation at the edge of the contact zone for low humidities (JKR-type contact) is replaced by rounded edges (DMT-type contact) with increasing humidity. This is predicted by the Maugis model and is experimentally observed using optical interference fringes of equal chromatic order. We are able to separate the capillary condensation and solid−solid contributions to the adhesive force because the Maugis model allows a direct calculation of the area on which the Laplace pressure acts. At humidities approaching saturation the forces due to capillary condensation dominate monolayer−monolayer adhesion. At lower humidities both capillary condensation and direct monolayer−monolayer interaction contribute to the overall adhesion.

Introduction

Organic self-assembled monolayers (SAMs) can be used to alter and control the chemical nature of surfaces. Self-assembly is simple and widely applicable in areas such as coatings, lubrication, templating, optoelectronics, and microelectromechanical systems (MEMS). The alkylsilanes form SAMs and have attracted attention because they are capable of cross-polymerization and covalent attachment to SiO_2-based oxide surfaces such as oxidized silicon wafers. Mica also contains Si−O bonds, but there are no inherent functional groups on the surface. SAMs on mica are potentially useful in nonlinear optics because mica can be prepared as relatively large, molecularly smooth sheets.[1]

Despite the lack of functionality, several research groups have investigated the deposition of alkylsilanes, mostly *n*-octadecyltrichlorosilane (OTS) and *n*-octadecyltriethoxysilane (OTE), on mica.[2−17] These monolayers are hydrophobic as judged by the contact angle of water, but in some cases, the contact angle decreases with prolonged exposure to water.[4,17] Tian et al.[5] found that water penetrated into OTE SAMs deposited on mica, making the monolayers less stable in friction force measurements. In our recent work[17] we showed that OTE SAMs deposited on both untreated and plasma-treated mica are initially highly hydrophobic, but contact angle hysteresis indicated that water interacts favorably with the monolayers on prolonged exposure. Defects in the monolayer most likely make it possible for the water to reach the hydrophilic region between the silane headgroups and the mica. More water was adsorbed by the monolayers on untreated mica compared to the plasma-treated case. This work strongly indicated that if the SAM is not firmly anchored to the substrate, water can accumulate in the region between the SAM and the substrate. Near saturation, water droplets also condense on the surface presumably at monolayer defects regardless of how well the SAM is anchored. At very high humidities a capillary condensed annulus of water is observed around the contact zone.

In general, when two solid bodies come into contact they deform in a way which is determined by their elastic or viscoelastic properties, by the surface forces between them, and by any externally applied load.[18] Due to the practical importance of understanding interparticle adhesion, the relationship between surface deformation and adhesion has been studied extensively.[19,20] Maugis[21] gives an excellent historical overview of research in this area. Capillary condensation acts outside the contact area and modifies the adhesive force in two interrelated ways, first by altering the surface deformation and second by increasing the adhesive force due to the Laplace pressure in the annulus. In this work we consider the effect of humidity on both the deformation and adhesiveness of surfaces coated with hydrophobic monolayers that do not perfectly repel water.

While humidity apparently does not affect the adhesiveness of OTE SAMs on silicon[22] as measured with the atomic force microscope, Quon et al.[23] reported that humidity increased the adhesion between mica and a methyl-terminated SAM deposited on gold. Ohnishi et al.[24] found that capillary condensation contributes to adhesion between fluorinated silane SAMs on

* To whom correspondence should be addressed. E-mail: curry@ag.arizona.edu.
[†] University of Arizona.
[‡] The University of Leeds. E-mail: phy6hkc@phys-irc.novell.leeds.ac.uk.

10.1021/jp0265992 CCC: $25.00
Published on Web 03/27/2003

silica, whereas no capillary condensation was observed between the same monolayers deposited with the Langmuir−Blodgett technique. In studies of physisorbed surfactant monolayers on mica, Chen and Israelachvili[25] found that adhesion increased with relative humidity and was dependent on the hydrophilicity of the headgroups and phase state of the hydrocarbon chains. Humidity has also been shown to increase the mobility of surfactant molecules on the surface by penetrating into the headgroup region and weakening the attraction between the surfactant molecules and the mica.[25−27] Adhesion has mostly been studied by separating the surfaces, and simultaneous investigations of surface deformation and adhesion have been much less prevalent.

In this work we investigate the effect of humidity on the surface deformation and adhesion between plasma-treated and untreated mica surfaces coated with OTE SAMs. The surfaces are mounted on crossed cylinders in the surface forces apparatus (SFA).[28,29] This geometry is equivalent to a sphere interacting with a flat surface. The SFA is particularly well suited for these experiments since the interferometric technique allows direct observation of the surface shape and size of the contact zone. In the presence of a capillary condensed liquid bridging the two surfaces, the measured adhesive force has contributions both from the direct solid−solid adhesion and from the Laplace pressure arising from the liquid−vapor interface.[30] If the surfaces are wetted by the vapor (i.e., small contact angle), a thin film of liquid is adsorbed on the surfaces in undersaturated conditions. Increased vapor pressure leads to thicker films.[31,32] If the surfaces then make contact, it is very difficult to force the last layers of liquid out of the contact zone in order to achieve molecular contact. This has been shown to significantly reduce the contribution of the solid−solid attraction to the adhesive force.[33,34] In this work the advancing and receding contact angles of water on the OTE SAM are 102° and 35°, respectively, if the mica substrate is untreated and are 107° and 75° if the substrate is plasma-treated prior to coating. The solid−solid adhesive force is hence potentially important even at high humidities because water is expelled from between the surfaces when they adhere, allowing molecular contact. Water capillary condenses around the surfaces even though these are not water-wet, presumably due to the presence of more hydrophilic defects. This means that at humidities near saturation both capillary condensation and solid−solid interactions may contribute to the adhesive force.

The geometry of the capillary condensate is related to the vapor pressure by the well-known Kelvin equation[35]

$$\frac{kT}{v_m}\ln\frac{p}{p_0} = \gamma_{LV}\left(\frac{1}{r_1}+\frac{1}{r_2}\right) \tag{1}$$

where r_1 and r_2 are the meniscus radii of curvature, γ_{LV} is the liquid−vapor surface tension, p/p_o is the vapor pressure, and v_m is the molar volume of the condensed liquid. In the case of two crossed cylinders of macroscopic radii R, the capillary condensate around the contact zone has $R \gg r_1$, r_2 and $r_2 \gg r_1$. Equation 1 then reduces to

$$\frac{kT}{v_m}\ln\frac{p}{p_0} = \frac{\gamma_{LV}}{r_k} \tag{2}$$

where r_k ($=r_1$) is the Kelvin radius. The Young−Laplace equation relates the pressure difference Δp across a curved interface to the surface tension and local meniscus curvature as follows:

$$\Delta p = \frac{\gamma_{LV}}{r_k} \tag{3}$$

From simple geometrical arguments it can be shown[30] that for nonadhesive contact between a rigid sphere and a rigid flat plate the adhesive force due to the Laplace pressure acting on an area A is equal to

$$F_S = \Delta p \times A = 4\pi R\gamma_{LV}\cos\theta \tag{4}$$

where R is the radius of curvature of the surface and θ is the receding contact angle of the liquid on the solid. This equation is also directly obtained from the Derjaguin approximation. It can also be shown that this equation holds even if the sphere is deformable as long as the contact is nonadhesive (Hertzian) so that the deformation δ is given by

$$\delta = \frac{a^2}{2R} \tag{5}$$

where a is the radius of the flattened contact area (see Figure 1). In this case the surface area acted upon by the Laplace pressure is

$$A = \pi(\rho^2 - a^2) \tag{6}$$

where ρ is the distance from the center of the contact to the three phase line as shown in Figure 1. Simple geometrical arguments give

$$\rho^2 = 2R(d+\delta) \tag{7}$$

and

$$d = 2r_k\cos\theta \tag{8}$$

where δ is the deformation and d is as indicated in Figure 1. Using eqs 5, 7, and 8 in eq 6, it can be seen that the adhesive force is still given by eq 4, which shows that deformation does not influence the adhesive force due to capillary condensation if the contact is Hertzian. Christenson[36] apparently verified this for capillary condensed cyclohexane, *n*-hexane, and water in the SFA. He found that in the high relative vapor pressure regime the pull-off force, which is the negative of the adhesive force, is in most cases given mainly by the Laplace pressure contribution to the adhesion as given by eq 5. This was valid for vapor pressures down to at least $p/p_o \sim 0.7$, even though separation at the lower end of the range did take place with a finite and large contact diameter. The surfaces were brought into contact in vapors that wetted the surfaces most likely reducing the solid−solid contribution to the adhesive force as discussed above. In the case of water condensing between H^+−mica surfaces, however, the adhesive force was greater than the Laplace pressure contribution and the solid−solid contribution was clearly identifiable.

Equation 4 predicts that the adhesive force due to capillary condensation is independent of vapor pressure. This is because as the vapor pressure is lowered the volume of condensate decreases but the curvature of the interface increases leading to the same effective capillary force. This however does not make physical sense at low vapor pressures since in that regime the adhesive force must be primarily dominated by solid−solid interactions. It is frequently pointed out that the Kelvin and Laplace equations must break down when the condensate radius approaches molecular dimensions; however, a quantitative

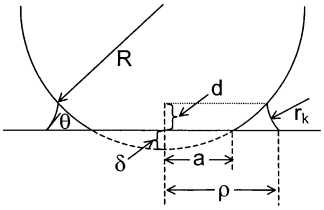

Figure 1. Schematic illustration of the geometry of the surfaces (the crossed-cylinder configuration is equivalent to a sphere on a flat). R is the radius of curvature of the surfaces (~2 cm), and θ is the contact angle of the liquid in a capillary condensate on mica. r_k is the Kelvin radius, δ is the deformation, a is the radius of the flattened contact area, and ρ is the distance from the contact center to the edge of the capillary condensate.

description of this breakdown has yet to appear. The Kelvin equation has in fact been verified for radii of curvature as small as 4 nm.[37]

If the sphere and flat are elastic and adhesive, the theory of K. L. Johnson, K. Kendall, and A. D. Roberts (JKR)[19] is frequently used to explain surface deformation and adhesion in dry conditions. The JKR theory predicts a finite contact diameter even under zero load. The adhesive force is given by

$$F_c = -\frac{3}{2}\pi RW = -3\pi R\gamma \tag{9}$$

where W is the Dupré energy of adhesion given by

$$W = \gamma_1 + \gamma_2 - \gamma_{12} \tag{10}$$

where γ_1 and γ_2 are the surface energies of the contacting materials and γ_{12} is the interfacial energy between the two surfaces. If the materials are identical, then $\gamma_{12} = 0$ and $W = 2\gamma$. The JKR theory only takes into account the adhesive interactions inside the contact zone and neglects interactions between the surfaces outside the contact zone. B. V. Derjaguin, V. M. Muller, and Yu. P. Toporov (DMT)[20] approached the problem from a different point of view, treating the contact as Hertzian but taking into account the interactions outside the contact zone. Their theory predicts an adhesive force of

$$F_c = -2\pi RW = -4\pi R\gamma \tag{11}$$

Maugis[21,38] showed that these two theories are actually special cases of a theory derived using linear elastic fracture mechanics with an adhesive "Dugdale" zone outside the contact area. In the Dugdale model a constant adhesive stress is assumed to act between the surfaces in a region just outside the contact zone. Outside this region the adhesive force falls to zero. Maugis found the system could be characterized by a parameter λ:

$$\lambda = \frac{2\sigma_o}{(\pi WK^2/R)^{1/3}} \tag{12}$$

where σ_o is the stress acting between the surfaces around the contact and the elastic constant (bulk modulus) K is given by

$$\frac{1}{K} = \frac{3}{2}\left(\frac{1-\nu^2}{E}\right) \tag{13}$$

where E is Young's modulus and ν is Poisson's ratio of the contacting materials. When the contacting bodies are large and elastic, the system parameter λ is large and JKR results are obtained. When the contacting bodies are small and rigid, λ is small and DMT results are obtained. We will show here that λ is also small for large elastic bodies in the presence of capillary condensation.

Fogden and White[39] gave a theoretical description of the effect of capillary condensation on adhesive forces in the Hertz theory. They outlined the procedure for adding capillary condensation to the JKR theory but did not further develop the theory. Maugis[38] pointed out that capillary condensation is the perfect example of a Dugdale zone outside the contact area. The condensate occupies an annulus in which the adhesive stress is constant and is given by the Laplace pressure. Maugis took the stress outside the contact zone to be

$$\sigma_0 = \Delta p \qquad a > r > \rho$$
$$= 0 \qquad r > \rho \tag{14}$$

where r is the radial coordinate. Maugis derived the following equations:

$$\frac{W}{\sigma_o} = \frac{a^2}{\pi R}((x^2-1)^{1/2} + (x^2-2)\tan^{-1}(x^2-1)^{1/2}) + \frac{16\sigma_o a}{3\pi K}((x^2-1)^{1/2}\tan^{-1}(x^2-1)^{1/2} - x + 1) \tag{15}$$

$$F = \frac{a^3K}{R} - 2\sigma_o a^2((x^2-1)^{1/2} + x^2\tan^{-1}(x^2-1)^{1/2}) \tag{16}$$

where $x = \rho/a$ and F is the load on the system. While it is not possible to simplify these equations further to obtain one equation that gives the load as a function of the contact radius, it is possible to solve these two equations using an iterative procedure. As shown in Maugis,[21] as $p/p_o \rightarrow 0$ JKR results are recovered and as $p/p_o \rightarrow 1$ DMT results are recovered.

Fogden and White[39] derived essentially the same equations except that instead of the first equation being equal to W/σ_o it is equal to $2r_k$. While both theories show that the adhesive force is given by eq 4 near saturation, at relative vapor pressures near zero the Fogden and White equations predict that the adhesive force is equal to $3\pi R\gamma_{LV}$ instead of $3\pi R\gamma_{SV}$, which is not in accord with most experimental observations.[39] Clearly the JKR equations should be recovered in dry conditions. We have used the Maugis model to analyze load as a function of contact radius for OTE−OTE adhesion at various humidities. Barthel et al.[40] used the model to interpret adhesive forces between silica surfaces. The deformation length instead of the contact radius was measured as a function of load due to system design. We have also measured the adhesive forces via the pull-off force method.

Experimental Section

OTE was purchased from Gelest, Inc. (Tullytown, PA) and doubly distilled under vacuum. Prior to self-assembly on untreated and plasma-treated mica the OTE was prehydrolyzed by dissolving 0.1 g of prefiltered OTE in 12 mL of THF containing 0.1 g of 1 N HCl. The solution was then stirred at room temperature for 2−3 days. Then 2.63 mL of the prehydrolysis solution was diluted with 80 mL of cyclohexane, resulting in a cloudy solution that was left to stand for 25 min. The solution did become clearer, but just prior to self-assembly, the hydrolyzed OTE solution was filtered through a 0.2 μm PTFE membrane filter. Filtering made the solution very clear, and there were no visible polymerized OTE aggregates at the air/solution interface. The OTE solution was slowly added to a clean jar containing a pair of either untreated or plasma-treated mica sheets that had been previously back silvered and glued

to cylindrically polished silica lenses. After 30 min, each mica surface was slowly and carefully removed from the solution and then baked in a vacuum oven for 2 h at 110 °C. Each sample was then rinsed with 3−5 mL of pure ethanol, blown dry with nitrogen, and immediately mounted inside the SFA chamber. A vial of P_2O_5 was attached to a port on the chamber exterior, and the chamber was purged with nitrogen for at least 4 h in order to scavenge any remaining water.

In some experiments the mica samples were pretreated with radio frequency generated Ar/H_2O plasma (Harrick plasma cleaner, PDC-3XG) in order to introduce hydroxyl functional groups on the surface prior to OTE self-assembly. The initial vacuum pressure in the plasma chamber was 100 mTorr. The vacuum pressure rose to 500 mTorr as a result of water vapor and argon gas (1.5 mL/min) introduction. The mica surfaces were positioned so that they faced directly into the argon/water vapor stream and were exposed to the plasma for 2 min at 30 W.

The experiments were carried out using a modified Mark IV SFA[28,29] with two OTE-coated, muscovite mica (plasma-treated or untreated) surfaces mounted as facing, crossed cylinders. The lower surface is mounted on either a flexible double cantilever spring [$k \sim 147$ N m^{-1}] or a stiff support [$k \sim 6.22 \times 10^3$ N m^{-1}], and the upper surface is mounted on a cylindrical piezoelectric crystal, the expansion of which controls the surface separation with an accuracy of 0.1 nm. Coarse surface separation was controlled directly with a dc motor on the translation stage attached to the lower surface, and fine control was achieved with the piezoelectric device attached to the upper surface. The mica (S & J Trading, NY) which had been cleaved into molecularly flat sheets (2−6 μm thick) and then back silvered was glued to cylindrically polished silica disks using an epoxy resin (Epon 1004, Shell Chemical Co.). The interferometer formed by the back-silvered surfaces transmits only certain discrete wavelengths that are passed through a diffraction grating and observed directly with an eyepiece as fringes of equal chromatic order (FECO) at the exit slit of the spectrometer. The fringes allow measurements of the surface separation and refractive index of the medium between the surfaces.[41] Before the plasma treatment or OTE coating, the contact fringe positions of the untreated mica surfaces were recorded for reference. The relative humidity was controlled by introducing 10−40 mL of an aqueous solution of known LiCl concentration into the bottom of the chamber. We allow 12 h for the system to come to equilibrium after the LiCl solution is injected into the chamber. The temperature near the OTE surfaces inside the SFA chamber was monitored with a thermistor and was maintained at 25.0 ± 0.1 °C throughout the experiment.

The adhesion or pull-off force is determined by bringing two OTE-coated mica surfaces into contact under zero external load and then separating them by moving the remote end of the spring on which one of the surfaces is mounted. When the resulting force on this surface equals the pull-off force the surfaces jump apart, and from the jump distance (measured from the fringes) and the spring constant the pull-off force is calculated.

Results and Discussion

The OTE-coated surfaces were brought into contact, and the contact radius as a function of applied load was measured first for increasing load and then for decreasing load (receding). The receding $a-F$ data for the OTE SAM on untreated mica as a function of relative humidity is shown in Figure 2. The surfaces jumped apart after measurement of the last data point. Data for the plasma-treated case are similar and are not shown. In the untreated case data for $p/p_o = 0$ (○), 0.80 (□), and 0.90 (△) are plotted in the upper panel of Figure 2. In the middle panels two sets of data obtained at different contact areas are shown for both $p/p_o = 0.95$ and 0.97. Data for $p/p_o = 0.99$ are shown in the lower panel. Equations 15 and 16 were used to obtain the theoretical fit to the data. The adhesive energy, W, was taken to be 2γ since the surface materials are identical and σ_o was determined from the vapor pressure according to eqs 2, 3, and 14. The fit was achieved by first selecting values for γ and K and solving eq 15 for x, which was then used in eq 16 to obtain the theoretical load as a function of the contact radius. The parameters γ and K were adjusted to yield the best fit to the experimental data as determined by a χ^2 test. The fitting parameters are listed in Tables 1 and 2 for the untreated and plasma-treated cases, respectively. K ranges from 1.9 to 3.4 × 10^{10} N/m^2, which is within the range of values previously obtained for the mica−glue system.[42,43] For $p/p_o = 0.99$ (untreated case) two fits are shown: in the first (solid line) all data points were used; in the second (dashed line) only the six points just prior to surface separation were fitted. The predicted surface energies are 62.5 mN/m (all points fit) and 54 mN/m (last six), indicating a variation in the fitting procedure does not produce wide variations in the predicted surface energy. The pull-off force, F_c, critical contact radius at pull-off, a_c, and the contact radius at zero load, a_0, were determined from the

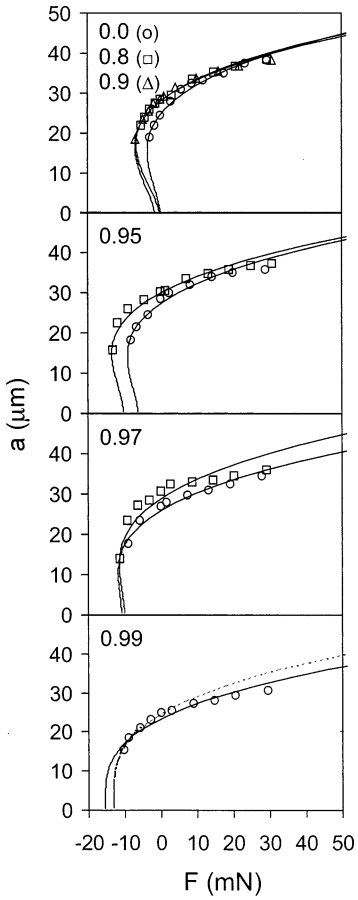

Figure 2. Load versus contact radius as the surfaces were gradually being pulled apart. The relative humidity is given in the upper left corner of each panel. Symbols for the top panel are $p/p_o = 0$ (○), 0.80 (□), and 0.90 (△). Solid lines are fits to the Maugis model. In the top panel the fits for $p/p_o = 0.80$ and 0.90 nearly coincide for large contact radii but differ slightly at small contact radii with the fit for $p/p_o = 0.80$ being closer to the $p/p_o = 0.0$ fit as the contact radius approaches zero. The dashed line in the lowest panel is an additional fit using only the six data points prior to surface separation.

TABLE 1: Theoretical Parameters for the OTE SAM on Untreated Mica[a]

p/p_o	γ (mN/m)	K ($\times 10^{-10}$ N/m^2)	F_c (mN)	a_c (μm)	ρ_c (μm)	a_0 (μm)	λ
0.0	18.5	1.9	−3.52	15.5	15.5	24.7	∞
0.80	34.5	2.3	−6.63	17.4	18.3	28.0	3.4
0.90	35.5	2.1	−6.96	16.7	19.9	28.0	1.7
0.95	43.5	2.2	−9.08	14.1	24.5	27.3	0.75
0.95	63	2.3	−13.36	14.7	28.6	29.9	0.65
0.97	52	1.9	−11.44	12.5	32.2	28.8	0.47
0.97	52.5	2.5	−11.79	10.3	31.8	25.9	0.39
0.99	62.5	3.0	−15.45	3.69	59.8	23.4	0.11
0.99	54	2.3	−13.22	4.71	55.4	19.9	0.13

[a] K, elastic constant; F_c, adhesive (pull-off) force; a_c, critical contact radius at pull-off; ρ_c, critical capillary condensate radius; a_0, contact radius at zero load; λ, Maugis parameter.

TABLE 2: Theoretical Parameters for the OTE SAM on Plasma-Treated Mica

p/p_o	γ (mN/m)	K ($\times 10^{-10}$ N/m^2)	F_c (mN)	a_c (μm)	ρ_c (μm)	a_0 (μm)	λ
0.0	20.3	2.0	−3.89	15.7	15.7	25.0	∞
0.0	24.7	2.8	−5.28	16.3	16.3	25.9	∞
0.80	21.1	2.5	−5.32	15.6	16.2	25.0	4.0
0.90	49.5	3.2	−11.15	16.3	21.9	28.5	1.2
0.90	53.5	3.4	−12.10	16.2	22.4	28.7	1.1
0.95	59.5	3.0	−14.35	13.7	28.9	28.8	0.58

fitted curves and are listed in Tables 1 and 2. Since the parameter x is determined by solving eq 15, we can also calculate ρ_c, the distance from the center of the contact to the edge of the meniscus at pull-off. This allows a calculation of the area on which the Laplace pressure acts.

The difference between the JKR and DMT pull-off force predictions (eqs 9 and 11) is the numerical factor of 3 or 4, respectively. Figure 3 shows $-F_c/\pi R\gamma$ as a function of relative humidity for OTE on untreated (○) and plasma-treated (□) mica. As relative humidity approaches zero, this quantity approaches 3 as is expected for JKR theory. As saturation is approached, this quantity increases toward 4, which is the value predicted by DMT theory. Qualitatively our observations support this transition. At low humidities the fringe corners are very sharp, indicating a JKR-type contact. At $\sim p/p_o = 0.95$ the fringe corners become rounded due to capillary condensation and the shape is closer to Hertzian. This has been observed in other work.[18,38] For $p/p_o \geq 0.97$ breaks in the fringes are observed as the surfaces are being separated, indicating a sizable capillary condensate.

The surface energy is by definition one-half the Dupré energy of adhesion, which is the energy required to separate unit areas of surface in another medium.[30] The medium varies from dry air to a near-saturated water vapor. The surface energy obtained from the theory is therefore the OTE SAM surface energy at various humidities. This is not the same as γ_{SV} or γ_{LV}, which are the limiting values in dry and near-saturated conditions, respectively. For the untreated case in dry conditions the surface energy is 18.5 mN/m, which is low compared to typically reported values.[3] Pull-off force measurements discussed below give the more typical value of 22 mN/m. In the plasma-treated case the average surface energy in dry conditions is 22.8 mN/m, which is consistent with published results.[3] As shown in Tables 1 and 2, the surface energy increases with increasing relative humidity as would be expected since water is adsorbed on the surface and the surface energy of the air−water interface is higher than that of the air−OTE interface. The question arises as to the reason for the water adsorption if the result is an increase in surface energy. A possible driving force is the

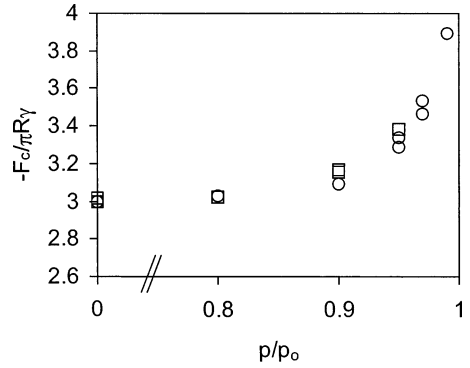

Figure 3. Predicted adhesive force divided by $\pi R\gamma$ as a function of relative humidity for OTE on untreated (○) and plasma-treated (□) mica.

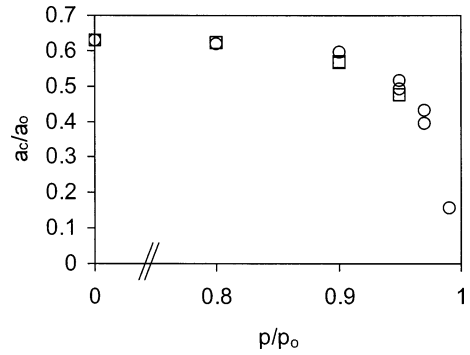

Figure 4. Predicted critical contact radius divided by zero load contact radius as a function of relative humidity for OTE on untreated (○) and plasma-treated (□) mica.

presence of defect sites on the surface where the local surface energy is higher than the average surface energy of the hydrocarbon surface. In previous work Christenson[36] found cyclohexane and *n*-hexane adsorption on potassium−mica lowered the surface energy whereas water adsorption on potassium−mica increased the surface energy.

Experimentally we observe that the size of the contact radius at pull-off or the critical contact radius, a_c, shrinks with increasing humidity. The model predicts that a_c is 15.5 μm at $p/p_o = 0.0$ and reduces to 3.7−4.7 μm at $p/p_o = 0.99$. The ratio of a_c to the contact radius at zero load, a_0, is plotted in Figure 4 for the untreated (○) and plasma-treated (□) cases. One of the results of JKR theory is that pull-off occurs at a finite contact radius and a particular a_c/a_0 ratio of ∼0.63. We find that the ratio is 0.63 at $p/p_o = 0.0$ as expected but decreases at higher humidities. DMT theory predicts the surfaces separate with zero contact radius. These data suggest the contact becomes more like a DMT contact with increasing humidity. The fact that the fringe corners become rounded at high humidities further supports this conclusion. The Maugis parameter, λ, is tabulated in Tables 1 and 2. At low humidities λ is large as expected for a JKR-type contact but with increasing humidity λ falls off dramatically even though the contacting materials are elastic with large radii of curvature. This shows that capillary condensation converts a JKR-type contact to a DMT-type contact.

At low relative humidity it is expected from physical considerations that adhesion is governed by solid−solid interactions and that at high relative humidity it is governed by capillary condensation. However, eq 4 predicts that the contribution to the adhesion from capillary condensation does not depend on humidity, implying this contribution is important even at low relative humidity. The Maugis model does not explicitly separate

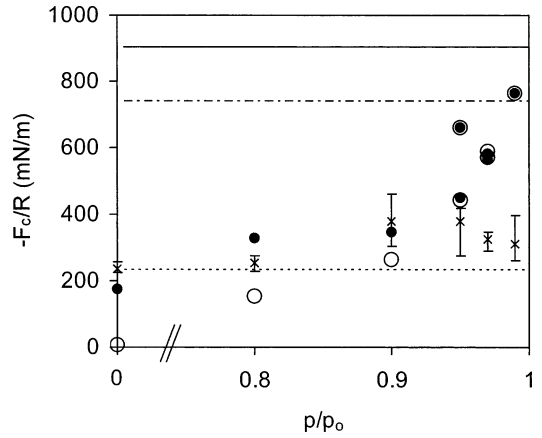

Figure 5. Normalized adhesive force for OTE on untreated mica as a function of relative humidity. The open and closed circles denote the Laplace pressure contribution to the adhesive force and the total adhesive force predicted from the Maugis model. Experimental pull-off force measurements are denoted by × symbols with error bars indicating the range of measured values. Horizontal lines denote the normalized adhesive force due to capillary condensation as calculated from eq 4 with $\theta = 0°$ (—), 35° (- — -), and 75° (---).

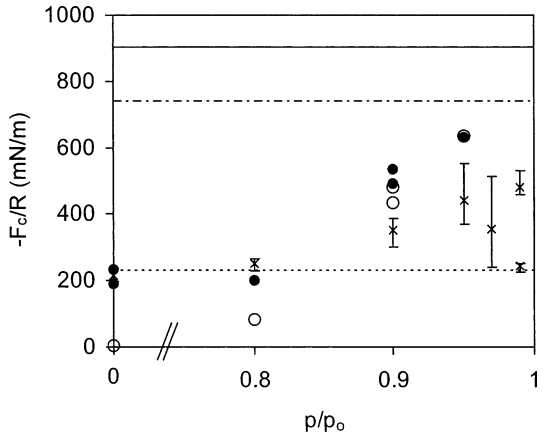

Figure 6. Normalized adhesive force for OTE on plasma-treated mica as a function of relative humidity. The open and closed circles denote the Laplace pressure contribution to the adhesive force and the total adhesive force predicted from the Maugis model. Experimental pull-off force measurements are denoted by × symbols with error bars indicating the range of measured values. Horizontal lines denote the normalized adhesive force due to capillary condensation as calculated from eq 4 with $\theta = 0°$ (—), 35° (- — -), and 75° (---).

the adhesive force into separate capillary condensation and solid−solid contributions; however, it is possible to directly test eq 4 because ρ_c and therefore the area of the surfaces covered by the condensate can be determined using eq 6. $\Delta p \times A$ can then be calculated directly to determine the humidity range where eq 4 applies. Figures 5 and 6 show the normalized adhesive force as a function of relative humidity for the untreated and plasma-treated cases, respectively. Closed circles are the total normalized adhesive force and larger open circles are the Laplace pressure contribution to the force ($\Delta p \times A$). The solid−solid contribution can be obtained by subtracting the Laplace pressure contribution from the total adhesive force. The experimentally measured pull-off forces (discussed below) are also shown (×) with error bars that give the range of the measured values. First, the adhesive force due to capillary condensation clearly depends on humidity. It decreases from the highest values near saturation to zero in dry conditions. This is not unexpected and has been shown previously.[36] It is expected, however, that eq 4 should hold at high humidities. To test this hypothesis, the contact angle of water on the OTE surfaces must be specified. In this work the receding contact angle of water on OTE-coated untreated and plasma-treated mica is 35° and 75°, respectively.[17] We choose the receding angle for this calculation because the meniscus recedes as the surfaces are being separated during the measurement. The horizontal lines in Figures 5 and 6 denote the normalized adhesive force due to capillary condensation as calculated from eq 4 with $\theta = 0°$ (—), 35° (- — -), and 75° (---), respectively. Considering first the untreated case, at $p/p_o = 0.99$ the total adhesive force, which equals the Laplace pressure contribution, is the same as the eq 4 prediction with $\theta = 35°$. This is consistent with the measured contact angle for untreated surfaces, suggesting that eq 4 holds at this humidity. More generally, the total adhesive force is the same as the Laplace pressure contribution for $p/p_o \geq 0.95$, suggesting that adhesion is dominated by capillary condensation at high humidities. However, even though the Laplace pressure dominates the adhesive force for $p/p_o \geq 0.95$, the adhesive force appears to decrease as the humidity decreases from $p/p_o = 0.99$ to 0.95. Equation 4 predicts that the adhesive force ($\Delta p \times A$) is constant and therefore independent of humidity. Since Δp is fixed by the vapor pressure, one can use eq 4 to determine the area which must be covered by the condensate to give a constant adhesive force for a given contact angle. For $p/p_o < 0.99$ the area covered by the condensate is less than that predicted by eq 4 with $\theta = 35°$. For $p/p_o \leq 0.90$ the solid−solid contribution becomes important, and at $p/p_o = 0.0$ the solid−solid contribution dominates the adhesion. In the plasma-treated case for $p/p_o = 0.95$ the Laplace pressure contribution is the same as the total adhesive force, indicating capillary condensation dominates adhesion at that humidity. Using the measured $\theta = 75°$ for the plasma-treated case, eq 4 predicts a much lower capillary condensation contribution to the adhesive force. The plasma-treated and untreated adhesive forces however are similar, suggesting the local contact angle is smaller than that measured in dynamic contact angle measurements. This is certainly possible given the surface heterogeneity.

Frequently the observation that the adhesive force due to capillary condensation decreases at low humidities is attributed to the fact that the size of the condensate approaches molecular dimensions, and therefore the macroscopic relations such as the Young−Laplace and Kelvin equations are no longer valid. Fisher and Israelachvili[37] have verified the Kelvin equation for condensates with a radius of curvature as small as 4 nm. Using eq 3, the Kelvin radius is 5 nm for $p/p_o = 0.90$. With $\theta = 35°$ the distance between the surfaces at the condensate edge is 4 nm. This would suggest that eq 4 should hold for $p/p_o \geq 0.90$. We find good agreement with eq 4 for $p/p_o = 0.99$ (untreated case); however, agreement falls off for lower humidities. It is not clear whether eq 4 holds for $p/p_o = 0.95$ and 0.97. There appears to be a decreasing trend in the Laplace contribution as the relative humidity decreases from 0.99; however, further work would be needed to establish the threshold for agreement with eq 4 quantitatively. This work outlines the method that could be used to accomplish this goal.

In separate experiments the pull-off force was experimentally measured as a function of relative humidity for OTE-coated untreated and plasma-treated mica. Each data point in Figures 5 and 6 is the average of several pull-off force measurements. The error bars denote the maximum and minimum measured values. Using JKR theory, the surface energy of the OTE monolayers at 0% relative humidity is calculated from the pull-off force according to eq 9 to be 22 and 25 mN/m for the plasma-treated and untreated cases, respectively. This is con-

sistent with literature reports.[3] At low humidities before capillary condensation is detectable, the pull-off forces agree well with the predicted adhesive forces determined from the force versus contact area measurements and the Maugis model. At high humidity the force versus contact area values are generally higher than the pull-off force measurements. It is not certain why there is disagreement at high humidities. The possibility that theory overestimates the adhesive force can be easily eliminated. A conservative estimate of the pull-off force can be obtained for $p/p_o = 0.99$ using the last measured point on the receding curve shown in Figure 2. The adhesive force normalized by the radius of curvature is still much larger, 510 mN/m, than the pull-off force measurements, showing the theory does not lead to this qualitative difference. It should be kept in mind that although both types of adhesion measurements involve pulling the surfaces apart the history of the surfaces prior to pull-off is different. In the force versus area measurements a load is applied to push the surfaces together before pulling them apart slowly, whereas in the pull-off force measurements the surfaces are separated more rapidly without applying an extra load. While it was expected, based on the measured receding contact angles, that the adhesive force in the untreated case would be much higher than that in the plasma-treated case, it is the measurement method that gives a difference in the adhesive force at high humidities. The surfaces are heterogeneous as evidenced both by the large dynamic contact angle hysteresis and by the fact that we see capillary condensation. Homogeneous surfaces would be very hydrophobic and would repel water. Surface heterogeneity leads to uncertainty in the local contact angle, which affects the adhesive force. It is not known how the local contact angle is affected by the surface separation method. Additionally, at high humidities it is possible that pull-off occurs after the surfaces are already separated by a small distance, as has been discussed in ref 36 and in earlier work on capillary condensation in liquid−liquid systems.[44] It is uncertain how this affects the pull-off force measurements compared to the force versus area measurements.

Concluding Remarks

Alkylsilane SAMs which are exceptionally stable and robust are routinely used to alter the chemistry of surfaces. Our previous work has shown that OTE SAMs deposited on mica are hydrophobic but can also absorb water from vapor most likely because of defects in monolayer packing that expose the underlying hydrophilic substrate. In this work we use the surface forces apparatus technique to investigate the effect of humidity on surface deformation and adhesion of plasma-treated and untreated mica surfaces coated with OTE SAMs. We use the Maugis model to analyze load as a function of contact radius for OTE−OTE adhesion at various humidities. We have also measured the adhesive force via the pull-off force method. The results with plasma-treated and untreated micas are not radically different because at high humidities capillary condensation, which is most likely due to monolayer defects, dominates in both cases. We find the Maugis parameter, λ, which is large for elastic bodies in dry conditions, decreases with increasing humidity, demonstrating how capillary condensation qualitatively changes the way elastic bodies in contact deform. In other words a JKR-type contact is converted to a DMT-type contact with increasing humidity. The surface energy and elastic constant were obtained as a function of humidity with γ_{SV} and γ_{LV} being the limiting values in dry and near-saturated conditions, respectively. Because the Maugis model allows a direct calculation of the area covered by the capillary condensate, we directly calculated the Laplace pressure contribution to the adhesive force as a function of humidity and found agreement with the well-known eq 4 at the highest humidities. This work outlines the method that could be used to establish the applicability of eq 4 in a more detailed study. We show that, even though the Maugis model does not treat the solid−solid and capillary condensation contributions to the adhesive force separately, it is possible to separate these contributions because the capillary condensate contribution can be determined directly.

Acknowledgment. This work was supported by the Petroleum Research Fund.

References and Notes

(1) Ulman, A. *An Introduction to Ultrathin Organic Films*; Academic: London, 1991.
(2) Kessel, C. R.; Granick, S. *Langmuir* **1991**, *7*, 532−538.
(3) Peanasky, J.; Schneider, H. M.; Granick, S.; Kessel, C. R. *Langmuir* **1995**, *11*, 953−962.
(4) Xiao, X. D.; Liu, G.; Charych, D. H.; Salmeron, M. *Langmuir* **1995**, *11*, 1600−1604.
(5) Tian, F.; Xiao, X.; Loy, M. M. T.; Wang, C.; Bai, C. *Langmuir* **1999**, *15*, 244−249.
(6) Parker, J. L.; Claesson, P. M.; Cho, D. L.; Ahlberg, A.; Tidblad, J.; Blomberg, E. *J. Colloid Interface Sci.* **1990**, *134*, 449−458.
(7) Parker, J. L.; Cho, D. L.; Claesson, P. M. *J. Phys. Chem.* **1989**, *93*, 6121−6125.
(8) Wood, J.; Sharma, R. *Langmuir* **1994**, *10*, 2307−2310.
(9) Wood, J.; Sharma, R. *Langmuir* **1995**, *11*, 4797−4802.
(10) Lambert, A. G.; Neivandt, D. J.; McAloney, R. A.; Davies, P. B. *Langmuir* **2000**, *16*, 8377−8382.
(11) Vallant, T.; Brunner, H.; Mayer, U.; Hoffmann, H.; Leitner, T.; Resch, R.; Friedbacher, G. *J. Phys. Chem. B* **1998**, *102*, 7190−7197.
(12) Schwartz, D. K.; Steinberg, S.; Israelachvili, J.; Zasadzinski, J. A. N. *Phys. Rev. Lett.* **1992**, *69*, 3354−3357.
(13) Nakagawa, T.; Soga, M. *Jpn. J. Appl. Phys.* **1997**, *36*, 6915−6921.
(14) Nakagawa, T.; Ogawa, K.; Kurumizawa, T. *Langmuir* **1994**, *10*, 525−529.
(15) Carson, G. A.; Granick, S. *J. Appl. Polym. Sci.* **1989**, *37*, 2767−2772.
(16) Carson, G. A.; Granick, S. *J. Mater. Res.* **1990**, *5*, 1745−1751.
(17) Kim, S.; Christenson, H. K.; Curry, J. E. *Langmuir* **2002**, *18*, 2125−2129.
(18) Horn, R. G.; Israelachvili, J. N.; Pribac, F. *J. Colloid Interface Sci.* **1987**, *115*, 480−492.
(19) Johnson, K. L.; Kendall, K.; Roberts, A. D. *Proc. R. Soc. London, Ser. A* **1971**, *324*, 301−313.
(20) Derjaguin, B. V.; Muller, V. M.; Toporov, Yu. P. *J. Colloid Interface Sci.* **1975**, *53*, 314−326.
(21) Maugis, D. *J. Colloid Interface Sci.* **1992**, *150*, 243−269.
(22) Xiao, X.; Qian, L. *Langmuir* **2000**, *16*, 8153−8158.
(23) Quon, R. A.; Ulman, A.; Vanderlick, T. K. *Langmuir* **2000**, *16*, 8912−8916.
(24) Ohnishi, S.; Yaminsky, V. V.; Christenson, H. K. *Langmuir* **2000**, *16*, 8360−8367.
(25) Chen, Y. L.; Israelachvili, J. N. *J. Phys. Chem.* **1992**, *96*, 7752−7760.
(26) Chen, Y. L. E.; Gee, M. L.; Helm, C. A.; Israelachvili, J. N.; McGuiggan, P. M. *J. Phys. Chem.* **1989**, *93*, 7057−7059.
(27) Berman, A. D.; Cameron, S. D.; Israelachvili, J. N. *J. Phys. Chem. B* **1997**, *101*, 5692−5697.
(28) Parker, J. L.; Christenson, H. K.; Ninham, B. W. *Rev. Sci. Instrum.* **1989**, *60*, 3135−3138.
(29) Israelachvili, J. N.; Adams, G. E. *J. Chem. Soc., Faraday Trans.* **1978**, *74*, 975−1001.
(30) Israelachvili, J. N. *Intermolecular and Surface Forces*, 2nd ed.; Academic Press: New York, 1991.
(31) Christenson, H. K. *J. Phys. Chem.* **1993**, *97*, 12034−12041.
(32) Curry, J. E.; Christenson, H. K. *Langmuir* **1996**, *12*, 5729−5735.
(33) Christenson, H. K.; Yaminsky, V. V. *Langmuir* **1993**, *9*, 2448−2454.
(34) Gee, M. L.; Israelachvili, J. N. *J. Chem. Soc., Faraday Trans.* **1990**, *86*, 4049−4058.
(35) Adamson, A. W. *Physical Chemistry of Surfaces*, 5th ed.; John Wiley & Sons, Inc.: New York, 1990.
(36) Christenson, H. K. *J. Colloid Interface Sci.* **1988**, *121*, 170−178.
(37) Fisher, L. R.; Israelachvili, J. N. *J. Colloid Interface Sci.* **1981**, *80*, 528−541.

(38) Maugis, D.; Gauthier-Manuel, B. *J. Adhes. Sci. Technol.* **1994**, *8*, 1311−1322.
(39) Fogden, A.; White L. R. *J. Colloid Interface. Sci.* **1990**, *138*, 414−430.
(40) Barthel, E.; Lin, X. Y.; Loubet, J. L. *J. Colloid Interface. Sci.* **1996**, *177*, 401−406.
(41) Israelachvili, J. N. *J. Colloid Interface Sci.* **1973**, *44*, 259−272.
(42) Chen, Y. L.; Helm, C. A.; Israelachvili, J. N. *J. Phys. Chem*. **1991**, *95*, 10736−10747.
(43) Christenson, H. K. *Langmuir* **1996**, *12*, 1404−1405.
(44) Christenson, H. K. *J. Colloid Interface. Sci.* **1985**, *104*, 234−249.